ACS APPLIED MATERIALS & INTERFACES

Research Article

www.acsami.org

In Vitro Study of Receptor-Mediated Silica Nanoparticles Delivery across Blood–Brain Barrier

Yang Song,[‡] Dan Du,[‡] Lei Li,[‡] Jun Xu,[§] Prashanta Dutta,*[,‡] and Yuehe Lin*[,‡]

[‡]School of Mechanical and Materials Engineering, Washington State University, Pullman, Washington 99164, United States

[§]Department of Integrative Physiology and Neuroscience, Washington State University, 1815 Ferdinand's Lane, Pullman, Washington 99164, United States

Supporting Information

ABSTRACT: A brain drug delivery system has been demonstrated by attaching lactoferrin (Lf) on the silica nanoparticles (Si NPs). The nanoparticle surface was modified with polyethylene glycol to reduce protein adsorption. The transport efficiency of Lf attached Si NPs was studied using an in vitro blood–brain barrier (BBB) model consisting of three distinct types of cells: endocytes, pericytes, and astrocytes. Transfer of NPs from the apical side to the basolateral side is observed. The results indicated that Lf attached Si NPs demonstrated enhanced transport efficiency across the BBB with size-dependence compared to bare Si NPs. The maximum transport efficiency of lactoferrin conjugated silica nanoparticle was observed for 25 nm diameter particles. This receptor-mediated transcytosis of Si NPs across the cerebral endothelial cells can be employed to deliver drugs and imaging probes to the brain.

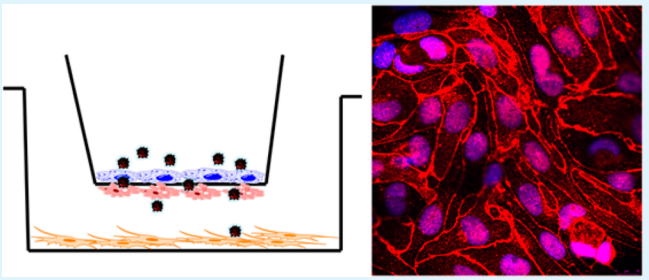

KEYWORDS: *silica nanoparticles, blood–brain barrier, receptor, lactoferrin, transcytosis*

INTRODUCTION

The fundamental role of the blood–brain barrier (BBB) is related with its precisely mediated transport between the body fluid and the central nervous system (CNS).[1−3] The BBB consists of specialized vascular endothelial cells (VECs), which exhibit extreme low expression of leukocytes binding molecules as well as tight junctions, which results in the limitation of paracellular transport.[4] The VECs can regulate transcellular transport by various vesicular transporters at the apical membranes. Only lipophilic molecules with low molecular weights could cross through the VECs via transcytosis and thus transport through the BBB freely, whereas other molecules are fully rejected by the BBB.[5] This distinct defense mechanism of the BBB effectively protects the CNS from the invasion of circulating toxins and harmful microorganisms.[6,7] However, the BBB also is a major obstacle for delivering new cerebral therapeutic agents to heal neurological disease.[1]

In past 2 decades, a number of drug delivery techniques have been tested for BBB with varying degree of success. Among various techniques, tight junction modulation, drug molecule modification, and nanoparticle-based transport approaches have led the drug delivery research. Drug delivery with tight junction modulations is reported using chemical and physical stimuli. Chemical stimuli take advantage of the osmotic opening of BBB by extracting water from VECs, which lead to alteration of their shape and as a consequence increased paracellular transport.[7] In physical stimuli, different physical mechanisms such as electromagnetic wave impingement,[8] magnetic nanoparticle invasion under alternating magnetic field, and microbubble-assisted focused ultrasound are used to locally and temporarily disrupt the BBB through deformation and restructuring of junction proteins.[9−11] Although various stimuli can potentially increase the penetration of agents to the CNS, high concentrations of these stimuli compounds can compromise brain function.[10] Moreover, microscopic and ultramicroscopic alterations of brain microvessel cells may lead to apoptosis.[12] On the other hand, the drug delivery through the modification of therapeutics is only possible for a very limited number of small molecules by lipophilization.[13] Even though the size of a drug molecule that can be transported is less than 500 Da, it is still possible to create temporary pores in the membrane bilayer.

To address the problem, we present the new drug carrier that can exploit endogenous transcytosis pathway for effectively delivering therapeutics without disrupting the normal function of BBB. In recent years, transcytosis across BBB has been demonstrated as a selective and noninvasive delivery mechanism.[7] Several receptor-mediated transcytosis (RMT) studies have been reported on the VECs with the aid of low-density lipoprotein receptor protein (LRP), transferrin receptor (TfR), and others. Moreover, a number of works took advantage of ligand-conjugation strategies on nanocarriers, such as lip-

Received: March 11, 2017
Accepted: May 25, 2017
Published: May 25, 2017

DOI: 10.1021/acsami.7b03504
ACS Appl. Mater. Interfaces 2017, 9, 20410−20416

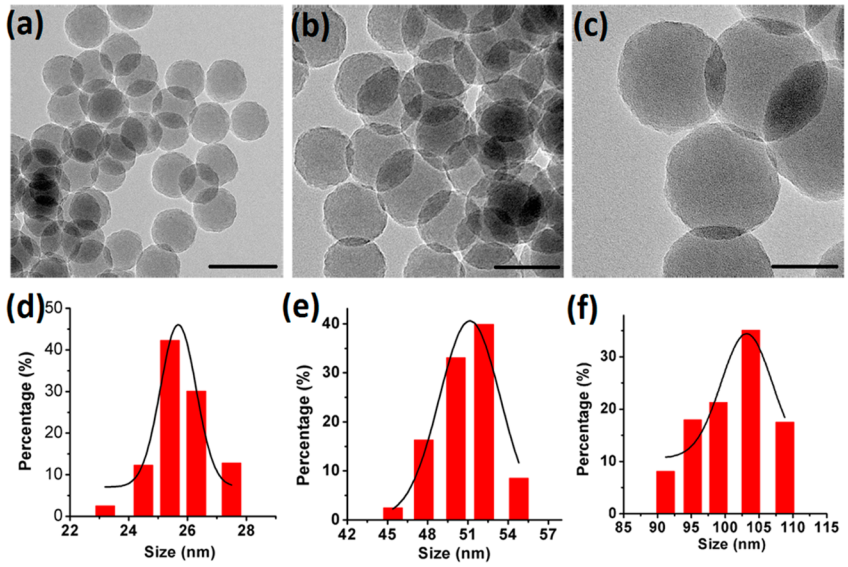

Figure 1. TEM images of (a) 25 nm, (b), 50 nm, and (c) 100 nm diameter Si NPs. Nanoparticle size distribution for (d) 25 nm, (e) 50 nm, and (f) 100 nm Si NPs. Scale bar: 50 nm.

osomes, polymeric nanoparticles, solid lipid nanoparticles, etc. to facilitate delivery of therapeutics and macromolecules across the BBB.[14−17] However, the poor delivery efficacy of these transport methods has not led to clinical translation, and hence new strategies are still required. Besides, these studies focus on the effect of specific ligands on their facilitation of cellular delivery, but the influences of size on transcytosis pathway and their combination (size effect and specific ligands) have not been addressed.

Silica nanoparticles (Si NPs) have attracted significant attention for their potential biomedical application compared to other nanomaterials, owing to their intrinsic properties, such as good biocompatibility, low cost, and manufacturing controllability.[18−23] These nanoparticles are generally recognized as safe by FDA and have been widely used in FDA approved food additive.[24,25]

Lactoferrin (Lf), a cationic iron-binding glycoprotein, is one of the promising candidates for targeting due to its relatively low cost, good biocompatibility, and high receptor-mediated transport efficiency.[26,27] The Lf receptors exist in human VECs of the BBB and can benefit Lf-mediated transcytosis through the in vitro BBB.[28−31] Moreover, due to the less endogenous concentration of Lf, it has been demonstrated that Lf ligands are better than commonly used transferrin ligands.[31,32] Here, we use fluorescence dye doped Si NPs functioned with Lf to transport across the BBB. Si NPs are coated with polyethylene glycol (PEG) to reduce protein adsorption, limit inflammation, and avoid invasion by reticuloendothelial system (RES). The PEG coating can also increase the blood circulation time of nanoparticles.[21,33−36] We specifically used three-cell coculture transwell system to study the BBB in vitro. This three-cell coculture system has been widely used to mimic the BBB phenotype, and hence it is an excellent in vitro platform to study the essential functions of BBB including permeability and transcytosis.

EXPERIMENTAL SECTION

Materials and Chemistry. Lactoferrin (Lf), Triton X-100, tris(2,2-bipyridyl)dichlororuthenium(II) hexahydrate (Rubpy), *n*-hexanol, tetraethyl orthosilicate (TEOS), 1-ethyl-3-[3-dimethylaminopropyl]carbodiimide hydrochloride (EDC), and *N*-hydroxysuccinimide (NHS) were ordered from Sigma-Aldrich (MA, USA). Bis-carboxy poly(ethylene glycol) (MW ≈ 10 kDa) was purchased from Nanocs (Tokyo, Japan). Collagen G, medium 199, DMEM medium, bovine calf serum, L-glutamine, gentamycin, penicillin, fetal bovine serum (FBS), and streptomycin were ordered from Gibco (MA, USA) to construct our in vitro BBB model.

Preparation of Silica Nanoparticles. Silica nanoparticles (Si NPs) were synthesized by using water-in-oil microemulsion method. Briefly, 3.75 mL of cyclohexane, 0.9 mL of Triton X-100, 0.8 mL of *n*-hexanol were mixed together. The mixture was diluted with different amounts of water (80, 200, and 560 μL) by stirring for 10 min. Then, 40 μL of 0.1 M Rubpy dye was added. Next, 100 μL of TEOS and 50 μL of NH_4OH were added to initiate polymerization. After a 24 h reaction, the nanocomposites were rinsed three times and then finally were freeze-dried to form a solid. To form Si NPs with primary amines, 10 μL of APTES was poured into the Si NPs solution (1 mg mL^{-1}) and then stirred for 20 h. The modified Si NPs were resuspended in MES solution after rinsing three times. 500 μL of EDC (0.05 mg mL^{-1}) and 500 μL of NHS (0.05 mg mL^{-1}) were then added to the as prepared solution and stirred for 1 h. Next, 600 μL of bis-carboxy-polythelene glycol (PEG) (100 $\mu g\ \mu L^{-1}$) was added and stirred overnight at 4 °C. The resulting PEG labeled Si NPs (PSi NPs) were washed with phosphate buffered saline (PBS) by centrifugation and dispersion in PBS.

Preparation of Lactoferrin Conjugated Si NPs. To increase the BBB penetration efficiency, lactoferrin (Lf) was attached to the PEG labeled Si NPs surface. The Lf conjugation procedure is as follows. First, EDC (2.5 $\mu g\ mL^{-1}$) and NHS (6.25 $\mu g\ mL^{-1}$) were dissolved in 950 mL of PEG labeled Si NPs solution. After about 30 min of stirring, an amount of 50 μL of 0.01 M PBS solution containing different amounts of Lf (150 μg for 25 nm Si NPs, 100 μg for 50 nm Si NPs, and 70 μg for 100 nm Si NPs) was introduced to trigger the reaction. The reaction continued overnight on ice. The as prepared PEG labeled Si NPs conjugated with Lf (PSi-Lf NPs) were collected and rinsed with water three times for removal of untreated Lf. The amount of Lf on the PSi-Lf NPs was quantified by the Bradford method. For the most consistent results, the reaction time of procedure was set to 10 min.

Trans-Endothelial Electrical Resistance Measurement. Light-phase imaging was used for morphological observation of the BBB model by phase contrast optical microscopy. The trans-endothelial electrical resistance (TEER) was measured to determine the integrity of the BBB model and development of tight junction. EVOM voltmeter (10 μA current at 12.5 Hz) with two detectors was applied

DOI: 10.1021/acsami.7b03504
ACS Appl. Mater. Interfaces 2017, 9, 20410−20416

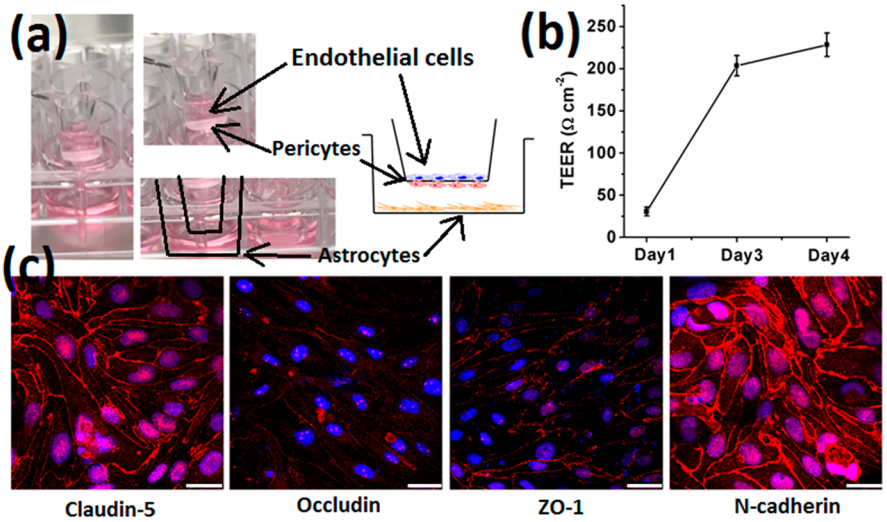

Figure 2. (a) Schematic representation of the in vitro model of BBB constructed from primary cultures of rat brain VECs, brain pericytes and astrocytes. (b) Transition of TEER after thawing until the start of the experiment. (c) Immunofluorescence of tight junction proteins (claudin-5, occludin, and ZO-1) and N-cadherin (red). Scale bar: 20 μm.

in this work, where the probe was placed in both the apical side and the basolateral side. The relative resistance value was recorded to calculate the TEER values by eq 1 as follows:

$$\text{TEER} = (R_t - R_b)^* A \quad (1)$$

where R_t and R_b represent the total resistance and background resistance, respectively, and A is the transwell area. The TEER value is directly correlated with the permeability of BBB for transport of extracellular molecule.[38]

Transport Efficiency of Nanoparticles. To evaluate the transport efficiency of PSi NPs or PSi-Lf NPs across the BBB model, desired concentrations of PSi NPs and PSi-Lf NPs were added to the apical side of the BBB models. Like TEER experiments, the blank culture medium was used as the control. After a 12 h incubation, the medium in the basolateral side was collected and analyzed by fluorescence spectrometry for the intensity of PSi-Lf NPs or PSi NPs. Since the fluorescence intensity of PSi NPs has a linear relationship with the concentration of NPs in the medium over the effective concentration range, the concentration of collective PSi NPs can be calculated accordingly. The transport efficiency of NPs across the BBB was calculated according to eq 2:

$$\text{transport efficiency}\,(\%) = \frac{M_b - M_c}{M_t - M_c} \times 100 \quad (2)$$

where M_b and M_t represent the collective concentration of transported NPs and the original medium containing 10 nM of NPs, respectively. M_c is calculated from autofluorescence of control medium.

RESULTS AND DISCUSSION

Nanoparticle Size Distributions. The transmission electron microscopy (TEM) images of different diameter Si NPs are shown in Figure 1a–c, while the nanoparticle size distributions are presented in Figure 1d–f as a histogram. As shown in Figure 1, the average diameters of silica nanoparticle were 26 ± 2, 53 ± 4, and 105 ± 5 nm. The ζ potential of different diameter silica nanoparticles was investigated before and after PEGlyation. The ζ potential values, as shown in Table S1 in Supporting Information, validated the PEGlyation of Si NPs. In addition, the PSi NPs exhibited great stability in both physiological saline and FBS, which is important for widespread use in biological applications.

As mentioned in the method section, the Bradford method was used for quantification of proteins in the purified PSi-Lf NPs. The protein assay results show that approximately 16.2, 69.5, and 284.7 Lf molecules were bound to 25 nm, 50 nm, and 100 nm PSi NPs, respectively. The measured protein contents on different size PSi NPs show almost similar Lf surface densities on all three size nanoparticles, which is approximately 0.0083 Lf nm^{-2}.

BBB Structure and Integrity. Many previous BBB studies have developed and used the monolayer cell culture system. Although the tight junction formed by the VECs is the fundamental structure of the BBB, a close cooperation between VECs and neighboring astrocytes and pericytes is required to regulate the function of the tight junction. Figure 2a shows the photographs of the in vitro coculture BBB system used in this study. Since the cells cultured in this model is derived from the rat brain capillary, this model can help us to study transcellular effects of the Lf because of its great similarities between rat and humans in vascular physiology. 4′,6-Diamidino-2-phenylindole (DAPI) staining is used to visualize three types of cell lines as shown in Figure S1. Furthermore, the tight junction and expression of proteins were examined with immunofluorescence methods, showing that the VECs grow closely and exhibited a spindle shaped physiological morphology (Figure 2c and Figure S2). Tight junctions can reduce transport across BBB by lowering the permeability due to expressed proteins including claudin-5, occludin, and ZO-1, etc. between VECs. Additionally, N-cadherin, an integral substrate residing in adhere junctions, facilitate cell–cell adhesion. Tight junction proteins and N-cadherin could act through their intimate association with the actin cytoskeletal network. From these aspects, as shown in Figure S3, N-cadherin protein was highly associated with actin networks due to the active regulation of cell polarity. Furthermore, the TEER value, an important parameter to evaluate the formation of tight junction by brain VECs, is shown in Figure 2b. This extremely high electric resistance value indicates the tight junctions between neighboring VECs, which could be higher than 200 Ω cm^{-2}.[37] The TEER value of the coculture BBB was sufficiently high to serve as a BBB in vivo.

Biocompatibility of Silica Nanoparticles. While nanoparticles are very suitable for drug delivery in different organs, the side effects of many NPs have been a major issue in

DOI: 10.1021/acsami.7b03504
ACS Appl. Mater. Interfaces 2017, 9, 20410–20416

nanomedicine. Thus, the biocompatibility of these synthesized nanoparticles is of paramount interest. Here biocompatibility refers to cytotoxicity and the functional integrity of BBB during transport of silica nanoparticles. The cytotoxicity of PSi NPs and PSi-Lf NPs has been evaluated using standard 3-(4,5-dimethylthiazol-2-yl)-2,5-diphenyltetrazolium bromide (MTT) assay with bEnd.3 cell. Over 93% cell viability is observed after incubation of bEnd.3 cell with either PSi NPs or PSi-Lf NPs of different sizes at the concentration ranging from 1 to 10 nM for 24 h (Figure S4), indicating the low cytotoxicity of PSi NPs and PSi-Lf NPs. Thus, PSi NPs and PSi-Lf NPs could be used as nanocarriers for transport through the in vitro BBB.

Nanoparticle Transcytosis Mechanism in Vitro. To test the hypothesis of nanoparticle transcytosis through the VECs, we first examined the intracellular mechanism of PSi-Lf mediated transcytosis. When PSi-Lf NPs were co-incubated with 10-fold excess free Lf, nanoparticles were successfully competed out (Figure 3a and Figure 3g). These results indicate that the uptake of PSi-Lf NPs requires the Lf receptor and the internalization occurs via the Lf receptor mediated pathway. To further assess the specific endocytosis pathway of PSi-Lf NPs, VECs were exposed to endocytic markers transferrin protein (Tf) and PSi-Lf NPs (Figure 3b) for 30 min. Here, PSi-Lf NPs showed efficient intercellular uptake and partial colocalization with Tf, indicating that postuptake PSi-Lf NPs are predominantly resident in the early endosomes (EEs). This result also confirms that during postendocytosis, PSi-Lf NPs follow the receptor mediated pathway. Next, we investigated the endocytosis specifically for PSi-Lf NPs by Lf receptor pathway. When cells were incubated for 60 min with Tf and PSi-Lf NPs, they exhibited significant colocalization (Figure 3c) revealing that PSi-Lf NPs had trafficked along the EEs or sorting endosomes (SEs). When the BBB was further incubated for 2 h and then labeled with Rab 5/Rab 7, it revealed that some PSi-Lf NPs had trafficked onward from EEs (Figure 4a). At the same time, PSi-Lf NPs containing compartment was confirmed to associate less with any of the late endosomes (LEs) (Figure 4b). Moreover, immunofluorescence methods were used to colocalize the PSi-Lf NPs with Rab11, which correspond to SEs. The PSi-Lf NPs were associated with the SEs with a high Pearson's coefficient, indicating most colocalization (Figure 3d). Z-stacks reconstructed CLSM imaging (Figure 3d) provided the extensive presence of PSi-Lf NPs in the transwell membrane pores, indicating that the PSi-Lf NPs were undergoing transcytosis. When BBB was labeled with Lyso-Tracker and PSi-Lf NPs for 4 h, most of the PSi-Lf NPs were trafficked backward from the LEs but not associated with any of lysosome, which was evidenced by a low Pearson's coefficient (Figure 3e and Figure 3h). The Z-stacks reconstructed 3D CLSM images further illustrate the nonacidifying lysosome pathway for the transcytosis (Figure 3f). Upon internalization, most PSi-Lf NPs were bonded and fused with EEs (Figure S5a). Small vesicles containing PSi-Lf NPs then emerged from the apical side and moved downward, constituting dynamic endosomes (Figure S5b). It is clear that a substantial portion of the PSi-Lf NPs has moved across the BBB approaching the basal side and end up at the transwell membrane pores so that the particles travel through the transwell pores (Figure S5c). In addition, with the counter-staining of the 3D model for VECs β-actin network, the PSi-Lf NPs were found to penetrate the VECs monolayer across its whole surface (Figure 4c). The tightness of our BBB model was enhanced by co-culturing pericytes. The transcytosis was still observed through the

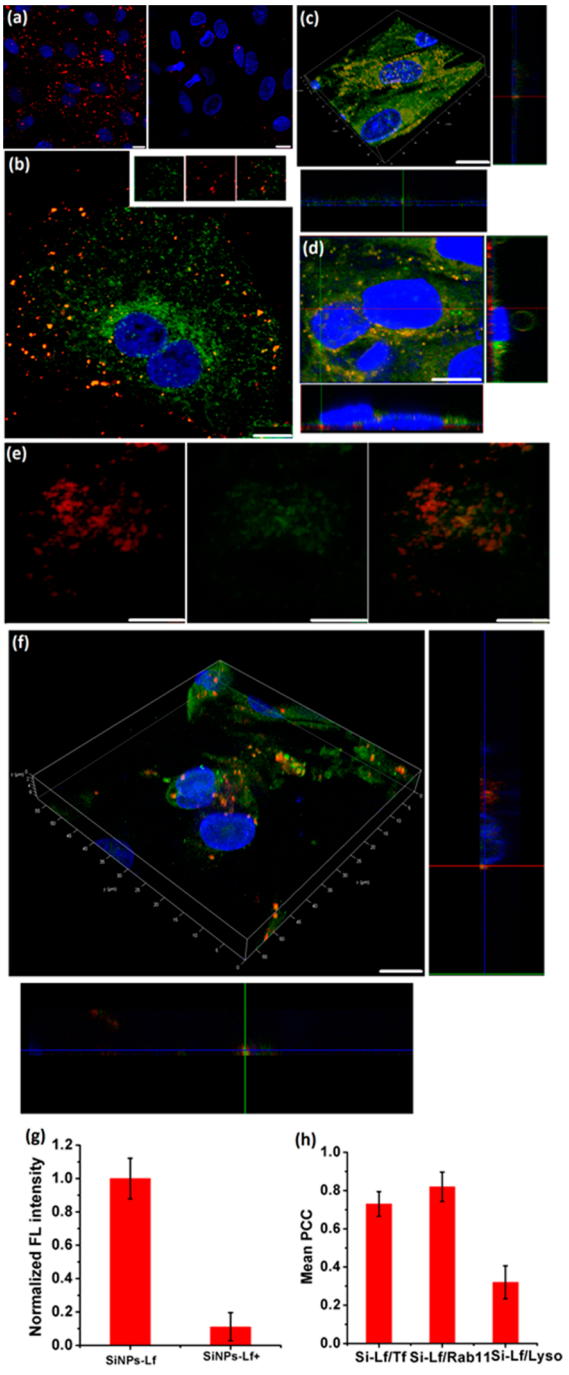

Figure 3. (a) Confocal images of the in vitro model of BBB treated with PSi-Lf NPs. Left: PSi-Lf NPs; Right: PSi-Lf NPs uptake in the presence of a 10-fold excess of Lf. (b) Cellular uptake of Tf (green) and PSi-Lf NPs (red) in in vitro model of BBB after 30 min of incubation at 37 °C. (c) Trafficking of PSi-Lf NPs along the Lf receptor pathway. Representative 3D confocal image showed colocalization of PSi-Lf NPs (red) and EE/SE marker Tf (green). (d) Representative 3D confocal image showed colocalization of PSi-Lf NPs (red) and SEs marker Rab-11 (green). (e) Colocalization study of PSi-Lf NPs (red) with Lyso-Tracker (green). (f) Z-stacks reconstructed into 3D images of colocalization profiles of PSi-Lf NPs (red) with Lyso-Tracker (green). (g) Relative fluorescence intensity analysis of cellular uptake of PSi-Lf NPs in Figure 3. (a). (h) Quantification of the colocalization of PSi-Lf NPs with Tf, Rab11, and LysoTracker. Mean Pearson's correlation coefficient (PCC) for $n = 30$ cells with the associated SD. Scale bar is 10 μm.

DOI: 10.1021/acsami.7b03504
ACS Appl. Mater. Interfaces 2017, 9, 20410−20416

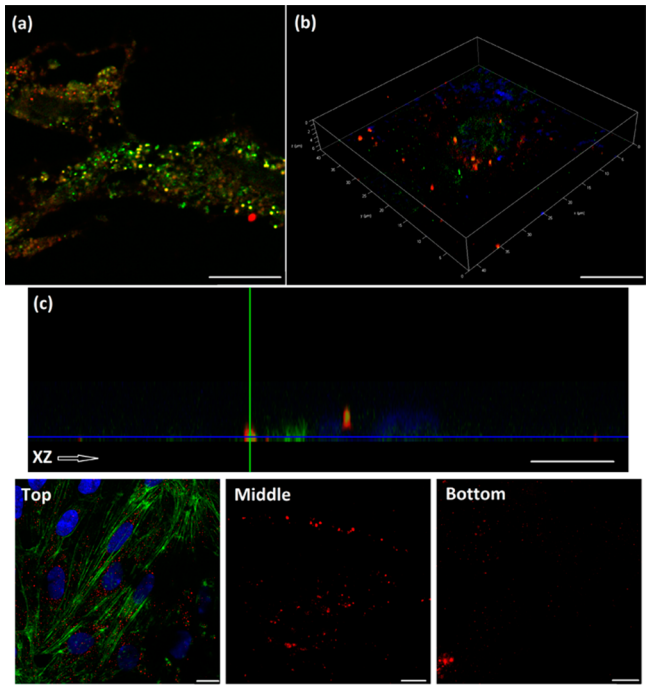

Figure 4. (a) Colocalization study of PSi-Lf NPs with Rab5 via immunocytochemistry in transwell inserts. (b) Colocalization study of PSi-Lf NPs with Rab7 via immunocytochemistry in transwell inserts. (c) Confocal images of the in vitro model of BBB treated with PSi-Lf NPs. (3D z-stack and top/middle/bottom single-plane confocal images). Scale bar is 10 μm.

different section, hence unlikely to be via paracellular transport through the tight junctions. These data indicated that the transcellular movement across the VECs monolayer is via an active receptor mediated mechanism rather than through passive diffusion.[39]

Nanoparticle Permeability across the in Vitro BBB. After a 12 h incubation of NPs at a concentration of 10 nM, the culture medium at the basolateral side was collected and analyzed for calculating the transport efficiency (using eq 2) to find the permeating ability of NPs across the in vitro BBB model. Generally, bare nanoparticles cannot effectively pass through the BBB, and our current results confirm that bare PSi NPs cannot pass through the BBB model. As shown in Figure 5c, the PSi NPs transport efficiencies are below 5% for diameter ranging from 25 to 100 nm. This poor transport efficiency in our in vitro BBB model can be attributed to the amphiphilic nature of PEG. In previous work, the barrier opening effect of Lf conjugated PEG-coated Fe_3O_4 NPs was presented.[29] Their in vivo results show that Lf can enhance the transport efficiency, but that study did not show any size effects. We systematically studied the size effects of ligand conjugated silica nanoparticles (PSi-NPs). The experimental results show that the particle size has a negative correlation for transport across the BBB: the 100 nm PSi-Lf NPs had the lowest transport efficiency of 5.8%, whereas the transport efficiency of 50 and 25 nm PSi-Lf NPs was 11.6% and 21.3%, respectively (Figure 5c). In other words, the maximum transport efficiency of PSi-Lf NPs was observed for 25 nm particles. In addition, confocal laser scanning microscopy (CLSM) was used to monitor eventual transcytosis after NPs exposure. The red fluorescence from the 25 nm PSi-Lf NPs revealed the most effective uptake by VECs, compared with 50 and 100 nm PSi-Lf NPs. The

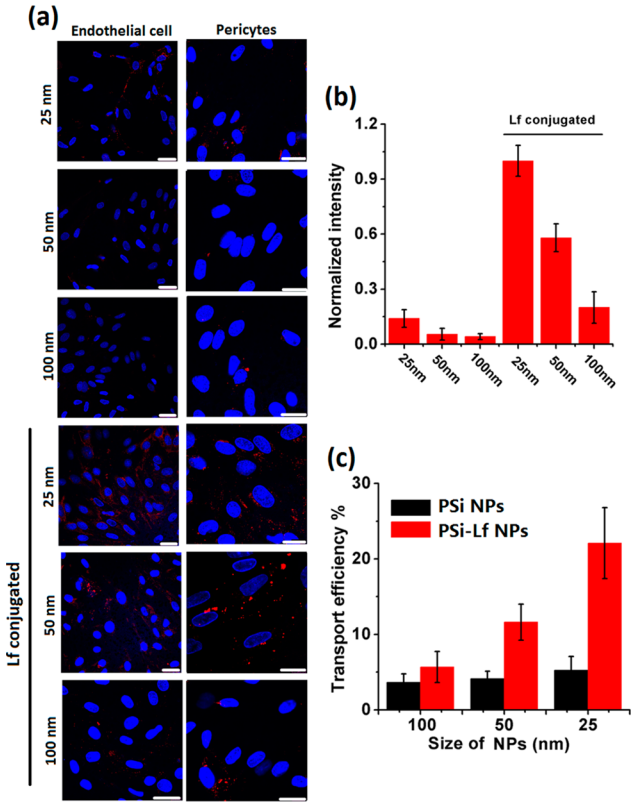

Figure 5. (a) Confocal fluorescence images of in vitro BBB model after incubation with 10 nM of (top three panels) PSi NPs and (bottom three panels) PSi-Lf NPs for 12 h. Results are presented for NPs size ranging from 25 to 100 nm. (b) Relative fluorescence intensity analysis of cellular uptake of various probes in endothelial cells. (c) Transport efficiencies of various probes across the in vitro BBB. Scale bar is 20 μm.

uptake of PSi NPs was strongly enhanced by conjugating Lf with NPs (Figure 5a and Figure 5b). These results indicate that cellular uptake of NPs by VECs not only is size-dependent but also heavily relies on the presence of the Lf. In the absence of Lf, the translocation of PSi NPs is not a strong function of nanoparticle size for this coculture BBB model. This result is in direct contradiction with the pervious in vitro work,[40] where they studied the translocation through a BBB formed from a single layer of ECs. Our studies clearly show that the three-layer BBB is much more resistant to particle translocation, and it is not possible to obtain meaningful transport efficiency without conjugating with the appropriate ligands.

Finally, to determine whether the PSi NPs and PSi-Lf NPs affected the normal function of BBB, we tested the permeability of BBB using sodium fluorescein (NaF). NaF cannot easily permeate through the BBB even if its molecular weight is low. Therefore, NaF can serve as the standard for assessing the permeability of BBB. The permeability test showed low apparent permeability coefficients (P_{app}) in all groups including those with PSi NPs and PSi-Lf NPs (Figure S6). This result indicates that the integrity of the BBB is still well maintained.

CONCLUSION

In summary, we successfully developed a brain drug delivery probe by covalently binding Lf to PSi NPs to achieve receptor-mediated delivery of NPs across the BBB. The in vitro BBB model experiments indicated that covalent binding with Lf

DOI: 10.1021/acsami.7b03504
ACS Appl. Mater. Interfaces 2017, 9, 20410−20416

favors the transfer of NPs across the BBB model. The transfer efficiency can be improved by reducing the particle size of PSi NPs. The current research further suggests that the PSi-Lf NPs could potentially be used as delivery vehicles for imaging and treatment of brain diseases by further coupling the NPs with diagnostic, therapeutic, and imaging agents with the aid of surface functionalized groups.

■ ASSOCIATED CONTENT

Supporting Information

The Supporting Information is available free of charge on the ACS Publications website at DOI: 10.1021/acsami.7b03504.

Experimental details, cellular cytotoxicity, immunostaining images, and permeability assay of BBB (PDF)

■ AUTHOR INFORMATION

Corresponding Authors

*P.D.: e-mail, prashanta@wsu.edu.

*Y.L.: e-mail, yuehe.lin@wsu.edu.

ORCID

Dan Du: 0000-0003-1952-4042

Yuehe Lin: 0000-0003-3791-7587

Notes

The authors declare no competing financial interest.

■ ACKNOWLEDGMENTS

This work was supported by the National Institute of General Medical Sciences of the National Institutes of Health under Award R01GM122081. The content is solely the responsibility of the authors and does not necessarily represent the official views of the National Institutes of Health.

■ REFERENCES

(1) Ballabh, P.; Braun, A.; Nedergaard, M. The Blood–Brain Barrier: An Overview: Structure, Regulation, and Clinical Implications. *Neurobiol. Dis.* **2004**, *16*, 1–13.

(2) Farrall, A. J.; Wardlaw, J. M. Blood–Brain Barrier: Ageing and Microvascular Fisease – Systematic Review and Meta-Analysis. *Neurobiol. Aging* **2009**, *30*, 337–352.

(3) Hawkins, B. T.; Davis, T. P. The Blood-Brain Barrier/Neurovascular Unit in Health and Disease. *Pharmacol. Rev.* **2005**, *57*, 173–185.

(4) Abbott, N. J.; Ronnback, L.; Hansson, E. Astrocyte-Endothelial Interactions at the Blood-Brain Barrier. *Nat. Rev. Neurosci.* **2006**, *7*, 41–53.

(5) Calvo, P.; Gouritin, B.; Chacun, H.; Desmaële, D.; D'Angelo, J.; Noel, J.-P.; Georgin, D.; Fattal, E.; Andreux, J. P.; Couvreur, P. Long-Circulating PEGylated Polycyanoacrylate Nanoparticles as New Drug Carrier for Brain Delivery. *Pharm. Res.* **2001**, *18*, 1157–1166.

(6) Begley, D. J. Delivery of Therapeutic Agents to the Central Nervous System: the Problems and the Possibilities. *Pharmacol. Ther.* **2004**, *104*, 29–45.

(7) Orive, G.; Ali, O. A.; Anitua, E.; Pedraz, J. L.; Emerich, D. F. Biomaterial-Based Technologies for Brain Anti-cancer Therapeutics and Imaging. *Biochim. Biophys. Acta, Rev. Cancer* **2010**, *1806*, 96–107.

(8) Gao, J.; Gu, H.; Xu, B. Multifunctional Magnetic Nanoparticles: Design, Synthesis, and Biomedical Applications. *Acc. Chem. Res.* **2009**, *42*, 1097–1107.

(9) Tran, N.; Webster, T. J. Magnetic Nanoparticles: Biomedical Applications and Challenges. *J. Mater. Chem.* **2010**, *20*, 8760–8767.

(10) Gupta, A. K.; Naregalkar, R. R.; Vaidya, V. D.; Gupta, M. Recent Advances on Surface Engineering of Magnetic Iron Oxide Nanoparticles and Their Biomedical Applications. *Nanomedicine* **2007**, *2*, 23–39.

(11) Neuberger, T.; Schöpf, B.; Hofmann, H.; Hofmann, M.; von Rechenberg, B. Superparamagnetic Nanoparticles for Biomedical Applications: Possibilities and Limitations of A New Drug Delivery System. *J. Magn. Magn. Mater.* **2005**, *293*, 483–496.

(12) Li, Z.; Barnes, J. C.; Bosoy, A.; Stoddart, J. F.; Zink, J. I. Mesoporous Silica Nanoparticles in Biomedical Applications. *Chem. Soc. Rev.* **2012**, *41*, 2590–2605.

(13) Lockman, P. R.; Mumper, R. J.; Khan, M. A.; Allen, D. D. Nanoparticle Technology for Drug Delivery Across the Blood-Brain Barrier. *Drug Dev. Ind. Pharm.* **2002**, *28*, 1–13.

(14) Lockman, P. R.; Koziara, J. M.; Mumper, R. J.; Allen, D. D. Nanoparticle Surface Charges Alter Blood–Brain Barrier Integrity and Permeability. *J. Drug Targeting* **2004**, *12*, 635–641.

(15) Schroeder, U.; Sommerfeld, P.; Ulrich, S.; Sabel, B. A. Nanoparticle Technology for Delivery of Drugs Across the Blood–Brain Barrier. *J. Pharm. Sci.* **1998**, *87*, 1305–1307.

(16) Yoshikawa, T.; Sakaeda, T.; Sugawara, T.; Hirano, K.; Stella, V. J. A Novel Chemical Delivery System for Brain Targeting. *Adv. Drug Delivery Rev.* **1999**, *36*, 255–275.

(17) Gidwani, M.; Singh, A. V. Nanoparticle Enabled Drug Delivery Across the Blood Brain Barrier: in Vivo and in Vitro Models, Opportunities and Challenges. *Curr. Pharm. Biotechnol.* **2014**, *14*, 1201–1212.

(18) Liu, D.; He, X.; Wang, K.; He, C.; Shi, H.; Jian, L. Biocompatible Silica Nanoparticles–Insulin Conjugates for Mesenchymal Stem Cell Adipogenic Differentiation. *Bioconjugate Chem.* **2010**, *21*, 1673–1684.

(19) Peng, J.; He, X.; Wang, K.; Tan, W.; Wang, Y.; Liu, Y. Noninvasive Monitoring of Intracellular pH Change Induced by Drug Stimulation Using Silica Nanoparticle Sensors. *Anal. Bioanal. Chem.* **2007**, *388*, 645–654.

(20) Santra, S.; Zhang, P.; Wang, K.; Tapec, R.; Tan, W. Conjugation of Biomolecules with Luminophore-Doped Silica Nanoparticles for Photostable Biomarkers. *Anal. Chem.* **2001**, *73*, 4988–4993.

(21) He, X.; Nie, H.; Wang, K.; Tan, W.; Wu, X.; Zhang, P. In Vivo Study of Biodistribution and Urinary Excretion of Surface-Modified Silica Nanoparticles. *Anal. Chem.* **2008**, *80*, 9597–9603.

(22) Singh, A. V. Editorial (Thematic Issue: Recent Trends in Nano-Biotechnology Reinforcing Contemporary Pharmaceutical Design). *Curr. Pharm. Des.* **2016**, *22*, 1415–1417.

(23) Singh, A. V.; Mehta, K. K. Top-Down Versus Bottom-Up Nanoengineering Routes to Design Advanced Oropharmacological Products. *Curr. Pharm. Des.* **2016**, *22*, 1534–1545.

(24) Peng, F.; Su, Y.; Wei, X.; Lu, Y.; Zhou, Y.; Zhong, Y.; Lee, S.-T.; He, Y. Silicon-Nanowire-Based Nanocarriers with Ultrahigh Drug-Loading Capacity for in Vitro and in Vivo Cancer Therapy. *Angew. Chem., Int. Ed.* **2013**, *52*, 1457–1461.

(25) Su, S.; Wei, X.; Zhong, Y.; Guo, Y.; Su, Y.; Huang, Q.; Lee, S.-T.; Fan, C.; He, Y. Silicon Nanowire-Based Molecular Beacons for High-Sensitivity and Sequence-Specific DNA Multiplexed Analysis. *ACS Nano* **2012**, *6*, 2582–2590.

(26) Huang, R.; Ke, W.; Liu, Y.; Jiang, C.; Pei, Y. The Use of Lactoferrin as A Ligand for Targeting the Polyamidoamine-Based Gene Delivery System to the Brain. *Biomaterials* **2008**, *29*, 238–246.

(27) Huang, R.; Ke, W.; Han, L.; Liu, Y.; Shao, K.; Jiang, C.; Pei, Y. Lactoferrin-Modified Nanoparticles Could Mediate Efficient Gene Delivery to the Brain In Vivo. *Brain Res. Bull.* **2010**, *81*, 600–604.

(28) Fillebeen, C.; Descamps, L.; Dehouck, M.-P.; Fenart, L.; Benaïssa, M.; Spik, G.; Cecchelli, R.; Pierce, A. Receptor-Mediated Transcytosis of Lactoferrin through the Blood-Brain Barrier. *J. Biol. Chem.* **1999**, *274*, 7011–7017.

(29) Qiao, R.; Jia, Q.; Hüwel, S.; Xia, R.; Liu, T.; Gao, F.; Galla, H.-J.; Gao, M. Receptor-Mediated Delivery of Magnetic Nanoparticles across the Blood–Brain Barrier. *ACS Nano* **2012**, *6*, 3304–3310.

(30) Hanada, S.; Fujioka, K.; Inoue, Y.; Kanaya, F.; Manome, Y.; Yamamoto, K. Cell-Based in Vitro Blood–Brain Barrier Model Can Rapidly Evaluate Nanoparticles' Brain Permeability in Association with Particle Size and Surface Modification. *Int. J. Mol. Sci.* **2014**, *15*, 1812–1825.

(31) Ji, B.; Maeda, J.; Higuchi, M.; Inoue, K.; Akita, H.; Harashima, H.; Suhara, T. Pharmacokinetics and BrainUptake of Lactoferrin in Rats. *Life Sci.* **2006**, *78*, 851−855.
(32) Huang, F.-Y.; Chen, W.-J.; Lee, W.-Y.; Lo, S.-T.; Lee, T.-W.; Lo, J.-M. In Vitro and in Vivo Evaluation of Lactoferrin-Conjugated Liposomes as a Novel Carrier to Improve the Brain Delivery. *Int. J. Mol. Sci.* **2013**, *14*, 2862−2874.
(33) Cheng, J.; Teply, B. A.; Sherifi, I.; Sung, J.; Luther, G.; Gu, F. X.; Levy-Nissenbaum, E.; Radovic-Moreno, A. F.; Langer, R.; Farokhzad, O. C. Formulation of Functionalized PLGA−PEG Nanoparticles for in Vivo Targeted Drug Delivery. *Biomaterials* **2007**, *28*, 869−876.
(34) Hak, S.; Helgesen, E.; Hektoen, H. H.; Huuse, E. M.; Jarzyna, P. A.; Mulder, W. J. M.; Haraldseth, O.; Davies, C. d. L. The Effect of Nanoparticle Polyethylene Glycol Surface Density on Ligand-Directed Tumor Targeting Studied in Vivo by Dual Modality Imaging. *ACS Nano* **2012**, *6*, 5648−5658.
(35) Singh, A. V.; Batuwangala, M.; Mundra, R.; Mehta, K.; Patke, S.; Falletta, E.; Patil, R.; Gade, W. N. Biomineralized Anisotropic Gold Microplate−Macrophage Interactions Reveal Frustrated Phagocytosis-like Phenomenon: A Novel Paclitaxel Drug Delivery Vehicle. *ACS Appl. Mater. Interfaces* **2014**, *6*, 14679−14689.
(36) Singh, A. V.; Raymond, M.; Pace, F.; Certo, A.; Zuidema, J. M.; McKay, C. A.; Gilbert, R. J.; Lu, X. L.; Wan, L. Q. Astrocytes Increase ATP Exocytosis Mediated Calcium Signaling in Response to Microgroove Structures. *Sci. Rep.* **2015**, *5*, 7847.
(37) Wong, A.; Ye, M.; Levy, A.; Rothstein, J.; Bergles, D.; Searson, P. The Blood-Brain Barrier: An Engineering Perspective. *Front. Neuroeng.* **2013**, *6*, 7.
(38) Lohmann, C.; Hüwel, S.; Galla, H. J. Predicting Blood-Brain Barrier Permeability of Drugs: Evaluation of Different in Vitro Assays. *J. Drug Target.* **2002**, *10*, 263−276.
(39) Tian, X.; Nyberg, S.; Sharp, P. S.; Madsen, J.; Daneshpour, N.; Armes, S. P.; Berwick, J.; Azzouz, M.; Shaw, P.; Abbott, N. J.; Battaglia, G. LRP-1-Mediated Intracellular Antibody Delivery to the Central Nervous System. *Sci. Rep.* **2015**, *5*, 11990.
(40) Liu, D.; Lin, B.; Shao, W.; Zhu, Z.; Ji, T.; Yang, C. In Vitro and in Vivo Studies on the Transport of PEGylated Silica Nanoparticles across the Blood−Brain Barrier. *ACS Appl. Mater. Interfaces* **2014**, *6*, 2131−2136.

DOI: 10.1021/acsami.7b03504
ACS Appl. Mater. Interfaces 2017, 9, 20410−20416